Wavelength-extended photovoltaic infrared photodetectors

Yan-Feng Lao, P. K. D. D. P. Pitigala, A. G. Unil Perera, L. H. Li, S. P. Khanna, and E. H. Linfield

Citation: Applied Physics Letters **104**, 131101 (2014); doi: 10.1063/1.4869958
View online: http://dx.doi.org/10.1063/1.4869958
View Table of Contents: http://scitation.aip.org/content/aip/journal/apl/104/13?ver=pdfcov
Published by the AIP Publishing

Wavelength-extended photovoltaic infrared photodetectors

Yan-Feng Lao,[1] P. K. D. D. P. Pitigala,[1] A. G. Unil Perera,[1,a)] L. H. Li,[2] S. P. Khanna,[2] and E. H. Linfield[2]
[1]*Department of Physics and Astronomy, Georgia State University, Atlanta, Georgia 30303, USA*
[2]*School of Electronic and Electrical Engineering, University of Leeds, Leeds LS2 9JT, United Kingdom*

(Received 4 February 2014; accepted 18 March 2014; published online 31 March 2014)

We report the incorporation of a long-wavelength photovoltaic response (up to 8 μm) in a short-wavelength *p*-type GaAs heterojunction detector (with the activation energy of $E_A \sim 0.40$ eV), operating at 80 K. This wavelength-extended photovoltaic response is enabled by employing a non-symmetrical band alignment. The specific detectivity at 5 μm is obtained to be 3.5×10^{12} cm Hz$^{1/2}$/W, an improvement by a factor of 10^5 over the detector without the wavelength extension. © *2014 AIP Publishing LLC*. [http://dx.doi.org/10.1063/1.4869958]

Photovoltaic detectors are attractive for achieving (i) extremely low noise, (ii) high impedance, and (iii) low power dissipation, compared to photoconductive detectors.[1] Various device concepts based on *p-n* junctions,[2] quantum well (QW),[3] quantum dot (QD),[4,5] type-II InAs/GaSb,[6] and quantum cascade (QCD) structures[5,7] have been explored to implement photovoltaic operation. One of the key factors is to have a built-in potential to sweep photocarriers out of the active region without an external field. Schneider *et al.*[3] reported a four-zone low-noise photovoltaic QW infrared photodetector (QWIP) with the preferable transport of carriers toward one direction. In a *n-i-p* type-II InAs/GaSb/AlSb detector,[6] internal electric field associated with the junction acts as the built-in asymmetry. Recently, Barve and Krishna[5] reported a photovoltaic QD infrared photodetector (QDIP) based on the QCD concept,[7] in which directional transfer of carriers between QDs is favored by cascade transitions through phonon coupling.

In addition to optimizing optical performance of the active region, the detectivity (D^*) of a detector is mainly limited by the dark current in photoconductive mode, or R_0A (R_0: zero-bias differential resistance, A: active area) in photovoltaic mode, which is determined by the activation energy (E_A). A detector operating in the longer wavelength range requires a reduced E_A, which typically lowers the detectivity, as a consequence of the increased dark currents and detector noise. In this Letter, we report a detector capable of operating up to 8 μm in the photovoltaic mode, while having the R_0A value determined by $E_A = 0.40$ eV. This means that the R_0A value is significantly greater than a conventional 8-μm threshold detector (which has the activation energy of 0.155 eV). Improvement by a factor of $\sim 10^7$ in D^* is thus expected from the R_0A improvement. Experimentally, D^* of the 8-μm threshold single-emitter detector reported here is 10^5 times higher than that of a previously reported 30-period detector.[8]

The detector architecture uses the standard structure of internal-photoemission detectors,[8] in which a highly *p*-type doped GaAs acts as the photon absorber and emitter. Figure 1(a) shows the valence band, which has a non-symmetrical band configuration. In addition to an offset (δE_v) between the barriers below and above the emitter, one of the AlGaAs barriers is graded to further increase the non-symmetry, and facilitate the transport of photoexcited holes at zero bias. The room-temperature photovoltaic operation has been reported elsewhere.[9] For comparison, different gradients of Al fractions [i.e., x varies from 0.45 to 0.75, or remains a constant (Table I)] were investigated. Figure 1(b) schematically shows the inter-valence band (IVB) transitions mainly responsible for photon absorption and hole escape over the barrier (through internal photoemission). To determine E_A, the characteristics of dark current-voltage-temperature (I-V-T) were measured, as shown in Fig. 2(a). Fig. 2(b) plots R_0A values extracted from I-V-T data, where a previous symmetrical GaAs/$Al_{0.57}GA_{0.43}$As detector (sample SP3)[10] is also shown for comparison. The Arrhenius plots are used to fit R_0A and determine E_A to be 0.37, 0.40, and 0.49 eV for samples SP1005, SP1007, and SP1001 (Table I), respectively. Except for SP1001, the obtained E_A values are comparable to the designed internal work function (Δ) of $\sim$0.40 eV, in accordance with the *p*-type GaAs/$Al_{0.75}Ga_{0.25}$As junction by taking into account *p*-type-doping effects.[11] The R_0A-T characteristic giving $E_A \sim 0.4$ eV demonstrates that both SP1005 and SP1007 behave like a 3-μm threshold detector.

The photovoltaic responsivity and detectivity (D^*) at 80 K are shown in Figs. 3(a) and 3(b), respectively. Spectral

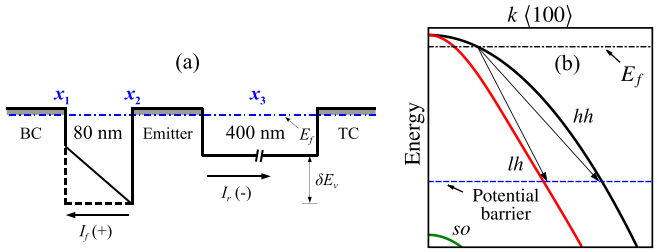

FIG. 1. (a) The valence-band diagram of a graded (solid line)/flat (dashed line) barrier structure. Bidirectional photocurrents can simultaneously exist in the sample for photovoltaic operation, as shown by $I_f(+)$ and $I_r(-)$, corresponding to forward and reverse photocurrents, respectively. x_1, x_2, and x_3 are the Al fractions of the barriers as described in Table I. δE_v is an offset between the barriers below and above the emitter. (b) Schematic of optical transitions between two valence bands, i.e., the heavy-hole (HH) and light-hole (LH) bands. For holes to escape over a potential barrier, optical transitions typically occur with the assistance of phonons.

a)uperera@gsu.edu

TABLE I. GaAs/$Al_xGa_{1-x}As$ photovoltaic detector parameters. The active region (from top to bottom) consists of a 400 nm-thick undoped $Al_{x_3}Ga_{1-x_3}As$ barrier with constant x_3, a *p*-type GaAs layer (emitter) doped to $1 \times 10^{19}\,cm^{-3}$, and a flat (SP1001) or graded (SP1005 and SP1007) 80 nm-thick $Al_xGa_{1-x}As$ barrier (x varies from x_2 to x_1). Figure 1(a) shows the valence-band diagram. d_e, E_A, and λ_T denote the thickness of emitter, activation energy, and the threshold wavelength of photovoltaic response, respectively.

Sample no.	x_1	x_2	x_3	d_e (nm)	E_A (eV)	λ_T (μm)
SP1001 (flat-barrier)	0.75	0.75	0.57	80	0.49	3.9
SP1005 (graded-barrier)	0.45	0.75	0.57	20	0.37	8.0
SP1007 (graded-barrier)	0.45	0.75	0.57	80	0.40	8.0

response was measured by a Perkin-Elmer system 2000 Fourier transform infrared spectrometer. The dimension of the sample is $400 \times 400\,\mu m^2$ mesas, with an area of $260 \times 260\,\mu m^2$ opened in the center allowing for front-side illumination. A bolometer with known sensitivity is used for background measurements and calibration of the responsivity. D^* was obtained[6] by using $D^* = \mathcal{R}/(2qJ + 4kT/R_{diff}A)^{1/2}$, where $\mathcal{R}$ is the responsivity, J is the dark current density, and R_{diff} is the differential resistance. At zero bias where the shot noise vanishes, this expression is reduced to the normal form in terms of the Johnson noise.[4] With decreasing temperature, R_{diff} rapidly increases for the bias around 0 V. To calculate photovoltaic D^* at 80 K, extrapolation of R_0 in terms of the Arrhenius plots [Fig. 2(b)] has been carried out.

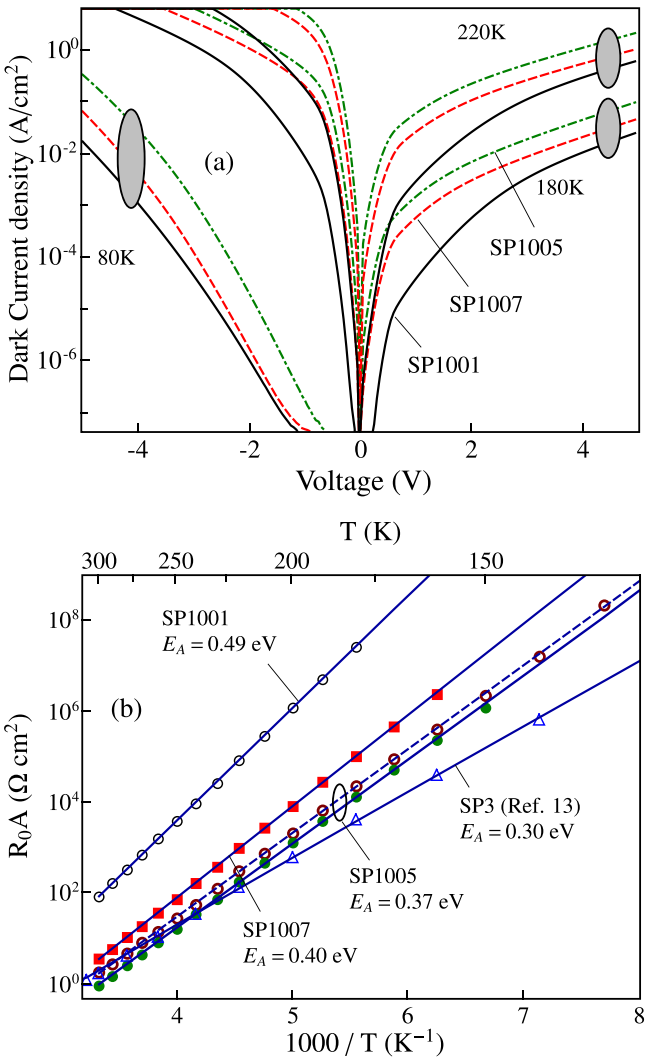

FIG. 2. (a) Dark I–V characteristics at different temperatures. (b) The Arrhenius plots of R_0A against 1000/T, to determine the activation energies (E_A). All of data result from measurements of $400 \times 400\,\mu m^2$ mesas, except for SP1005, for which an additional device with the dimension of $800 \times 800\,\mu m^2$ (open circles) is plotted to confirm the consistency. Also shown is a previously reported[10] symmetrical flat-barrier detector (SP3), which has the zero barrier offset, i.e., $\delta E_v = 0$ eV. Its E_A corresponds to the activation energy of the *p*-type GaAs ($3 \times 10^{18}\,cm^{-3}$)/$Al_{0.57}Ga_{0.43}As$ junction.

An interesting feature in the spectral response of the graded-barrier samples is the large redshift in the threshold wavelength under photovoltaic operation (doubling the operating wavelength range). From the photoresponse characteristic point of view, the device with $E_A \sim 0.40$ eV acts as an 8-μm threshold detector. Notice that the flat-barrier sample SP1001 does not respond beyond 3.9 μm, which is similar to the symmetrical GaAs/$Al_{0.57}Ga_{0.43}As$ detector as observed before (sample SP3).[10] Another feature being observed is the zero-responsivity point lying between 3.4 and 3.5 μm, which is an indication of bidirectional photocurrents simultaneously existing in the sample [see Fig. 1(a)]. This can be understood since photoexcited holes in the emitter can emit over both sides of the barriers, which normally have the threshold wavelengths of 3 and 4 μm, corresponding to the heterointerfaces of GaAs/$Al_{0.75}Ga_{0.25}As$ and GaAs/$Al_{0.57}Ga_{0.43}As$, respectively. The photocurrent cancellation leads to the occurrence of zero response between 3 and 4 μm. Several zero-response points taking place in sample SP1001 are related to its band alignment with a flat barrier.

In general, threshold redshifting mostly results from bias-related effects, such as image-force barrier lowering and quantum tunneling. However, these effects are absent in the photovoltaic operating mode. A testimony of our observations was justified as being due to the high-energy photon excitation. Since the bottom contact (BC), emitter and top contact (TC) are highly doped, photoexcited holes can be created in all of these layers. Because of the graded barrier, high-energy photons can give rise to a net flow of photoexcited holes from BC to emitter. Some of the photoexcited holes are captured by the emitter. These high-energy captured holes tend to increase the energies of holes[12] originally in the emitter, and excite them to high-energy states. As a consequence, the energies of photons needed in order to excite holes to escape over the barrier can be correspondingly reduced, giving rise to a long-wavelength response. This process takes place in the hole transport from BC to TC, in agreement with observed wavelength-extended response corresponding to the reverse photocurrents (Fig. 3).

To justify the above mechanism, spectral response has been measured with the use of different long-pass filters (with the cut-on wavelength of λ_{CO}) and different intensities of incoming light, as shown in Fig. 4. This varies the energy or the concentration of photoexcited holes injected into the emitter. By using a filter with $\lambda_{CO} = 3.60$ μm, the short-wavelength response [labeled region 1 of Fig. 3] should disappear, as the escape of holes from the emitter to the BC cannot be accomplished because of the missing of the $h\nu > 0.34$ eV ($\lambda < 3.60$ μm) photons. For the same reason, photoexcited holes in the BC will be unable to overcome the

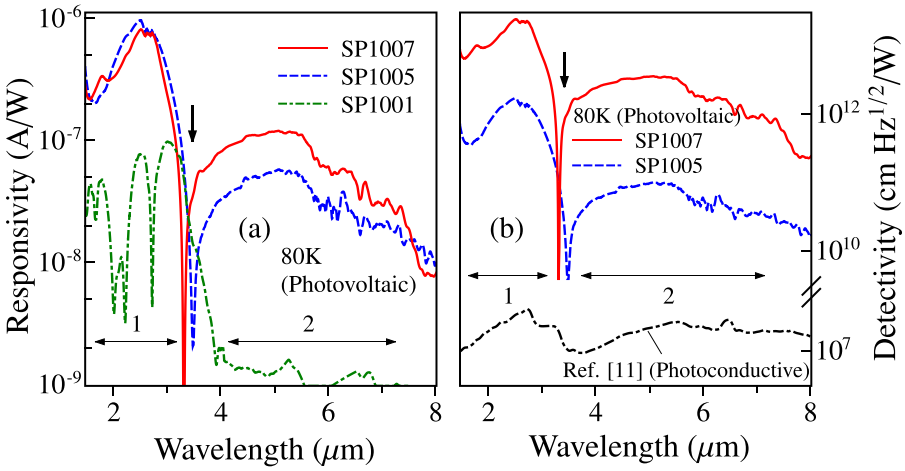

FIG. 3. The spectral (a) responsivity and (b) detectivity at 80 K. The vertical arrows indicate the occurrence of zero response due to bidirectional photocurrents simultaneously existing in the device, owing to the photovoltaic operating mode. Labeled response (1) and (2) correspond to the forward $[I_f(+)]$ and reverse $[I_r(-)]$ photocurrents. Long-wavelength response beyond 3.9 μm was not observed in flat-barrier sample SP1001. Table I summarizes the threshold wavelengths of photovoltaic response for three samples. The D^* value of SP1007 is 10^5 times higher than 30-period photoconductive detectors previously reported.[8]

graded barrier (highest barrier ~0.4 eV) to enter into emitter. This suppresses the long-wavelength response as well [labeled region 2 of Fig. 3], according to the aforementioned energy-transfer mechanism. As expected [Fig. 4(a)], photovoltaic response was unseen throughout the entire spectral range. In contrast, the use of a filter with $\lambda_{CO} = 2.40\,\mu$m gives rise to both short- and long-wavelength response owing to allowed emitter-to-BC and BC-to-emitter hole transport. The efficiency of energy transfer between photoexcited holes and holes in the emitter could be a critical factor determining the long-wavelength response. Such energy transfer results from carrier scatterings and could be subject to degradation from hole-impurity scattering as the emitter is highly doped. With increasing the concentration of photoexcited holes, enhanced hole-hole scatterings can be expected, leading to distinct response in long-wavelength range, as shown in Fig. 4(b). By calibrating the variation of the incoming light intensity, the short-wavelength portion of the response is expected to remain the same. However, the long-wavelength portion is almost negligible when the light intensity is reduced to 2.9%, and quickly rises up when the incoming light increases to 7.3%, where 100% of light corresponds to the default optical aperture in the experiment. This may also explain the response characteristic of sample SP1001 not beyond 3.9 μm, where because of the flat-barrier configuration the net injection of photoexcited holes from the BC to emitter is negligible.

Higher activation energy of the dark current-voltage characteristics than the photoresponse threshold energy can provide a significant improvement of the detector performance. According to $R_0A \sim \exp(-E_A/\mathrm{kT})$, the R_0A value (at 80 K) of our detector with $E_A = 0.40$ eV (responding up to 8 μm) is nearly 10^{15} times higher than a conventional detector with E_A of 0.155 eV (without wavelength extension, also responding up to 8 μm), which gives nearly 10^7 improvement in D^*. To experimentally evaluate the D^* improvement factor, same type of internal-photoemission detectors[8] was used, as shown in Fig. 3(b) (this detector contains 30 periods of emitters and barriers), which is nearly 10^5 times less than the present detector.

There are two main reasons causing the relatively low responsivity and thus low quantum efficiency (QE) in the present detector: the absorption of the emitter and lifetime of holes. The single-emitter structure only gives ~2% absorption efficiency, and thus can be improved at least by a factor of 10 using multiple periods. The fast carrier relaxation time (~0.1 ps) in $1 \times 10^{19}\,\mathrm{cm}^{-3}$ p-type doped GaAs is another

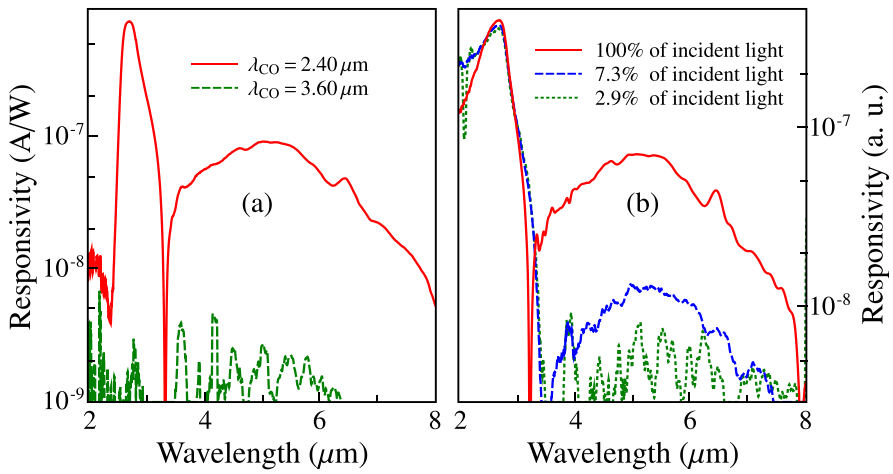

FIG. 4. (a) Photovoltaic response measured by using different long-pass filters (λ_{CO} is the cut-on wavelength). A filter with $\lambda_{CO} = 3.60\,\mu$m blocks the transport of photoexcited holes overcoming the graded-barrier region, thus suppressing both the short and long-wavelength response. (b) Variation of photovoltaic response with the intensities of incident light (through adjusting the optical aperture size of the spectrometer), where 100% of light corresponds to the default aperture size. The calibration of responsivity takes into account the variation of light, which leads to nearly unchanged responsivity values for the <3 μm wavelength range. The >3.5 μm response becomes almost negligible when the intensity of incoming light is reduced to 2.9%.

reason of low QE, which can be possibly improved by a factor of 10^4–10^8, by using quantum structures such as dots-in-well, which has the carrier lifetime in the nanosecond range.[13] Although demonstrated in heterojunction detectors, the wavelength-extension idea is based on the non-symmetrical band alignment and thus can be applied to detectors consisting of quantum structures. To conclude, the present study demonstrated a wavelength-extended photovoltaic detector with a significantly high R_0A value. This offers a possibility of incorporating long-wavelength response into a short-wavelength detector with the advantage of low dark-current operation.

This work was supported in part by the U.S. Army Research Office under Grant No. W911NF-12-2-0035 monitored by Dr. William W. Clark, and in part by the U.S. National Science Foundation under Grant No. ECCS-1232184. The University of Leeds acknowledges supports from the UK Engineering and Physical Sciences Research Council, and EHL from the European Research Council Advanced Grant "TOSCA". Authors acknowledge the contributions from Dr. H. C. Liu who was involved in this work, until his sudden death in October 2013.

[1]H. Schneider and H. C. Liu, *Quantum Well Infrared Photodetectors: Physics and Applications*, Optical Sciences, Vol. 126 (Springer, New York, 2007).
[2]A. Rogalski, Infrared Phys. Technol. **41**, 213 (2000).
[3]H. Schneider, C. Schönbein, M. Walther, K. Schwarz, J. Fleissner, and P. Koidl, Appl. Phys. Lett. **71**, 246 (1997).
[4]L. Nevou, V. Liverini, F. Castellano, A. Bismuto, and J. Faist, Appl. Phys. Lett. **97**, 023505 (2010).
[5]A. V. Barve and S. Krishna, Appl. Phys. Lett. **100**, 021105 (2012).
[6]A. M. Hoang, G. Chen, A. Haddadi, S. A. Pour, and M. Razeghi, Appl. Phys. Lett. **100**, 211101 (2012).
[7]F. R. Giorgetta, E. Baumann, M. Graf, Q. Yang, C. Manz, K. Köhler, H. E. Beere, D. A. Ritchie, E. Linfield, A. G. Davies, Y. Fedoryshyn, H. Jäckel, M. Fischer, J. Faist, and D. Hofstetter, IEEE J. Quantum Electron. **45**, 1039 (2009).
[8]Y. F. Lao, P. K. D. D. P. Pitigala, A. G. U. Perera, H. C. Liu, M. Buchanan, Z. R. Wasilewski, K. K. Choi, and P. Wijewarnasuriya, Appl. Phys. Lett. **97**, 091104 (2010).
[9]P. K. D. D. P. Pitigala, S. G. Matsik, A. G. U. Perera, S. P. Khanna, L. H. Li, E. H. Linfield, Z. R. Wasilewski, M. Buchanan, and H. C. Liu, J. Appl. Phys. **111**, 084505 (2012).
[10]P. V. V. Jayaweera, S. G. Matsik, A. G. U. Perera, H. C. Liu, M. Buchanan, and Z. R. Wasilewski, Appl. Phys. Lett. **93**, 021105 (2008).
[11]Y.-F. Lao and A. G. U. Perera, Phys. Rev. B **86**, 195315 (2012).
[12]S. G. Matsik, P. V. V. Jayaweera, A. G. U. Perera, K. K. Choi, and P. Wijewarnasuriya, J. Appl. Phys. **106**, 64503 (2009).
[13]M. R. Matthews, R. J. Steed, M. D. Frogley, C. C. Phillips, R. S. Attaluri, and S. Krishna, Appl. Phys. Lett. **90**, 103519 (2007).